HOKKAIDO UNIVERSITY

Mechanisms of current collapse and gate leakage currents in AlGaN/GaN heterostructure field effect transistors

Hideki Hasegawa,[a] Takanori Inagaki, Shinya Ootomo, and Tamotsu Hashizume
Research Center for Integrated Quantum Electronics and Graduate School of Electronics and Information Engineering, Hokkaido University, Sapporo, 060-8628, Japan

In order to clarify the mechanisms of drain current collapse and gate leakage currents in the AlGaN/GaN heterostructure field effect transistor (HFET), detailed electrical properties of the ungated portion and Schottky-gated portion of the device were investigated separately, using a gateless HFET structure and an AlGaN Schottky diode structure. The gateless device was subjected to plasma treatments and surface passivation processes including our novel Al_2O_3-based surface passivation. dc $I-V$ curves of gateless HFETs were highly nonlinear due to virtual gating by surface states. After drain stress, air-exposed, H_2 plasma-treated and SiO_2-deposited gateless HFETs showed an initial large-amplitude exponential current transient followed by a subsequent smaller, slow, and highly nonexponential response. The former was explained by emission from deep donors at $E_c-0.37$ eV, and the latter by emission from surface states. Capture transients with stress-dependent capture barriers were also observed. An x-ray photoelectron spectroscopy (XPS) study indicated that 0.37 eV-deep donors are N-vacancy related. On the other hand, no current transients took place in N_2 plasma treated and Al_2O_3-passivated samples. Temperature dependences of $I-V$ curves of Schottky diodes were extremely small and reverse currents were anomalously large. They were explained by the ''thin surface barrier'' (TSB) model where thermionic field emission and field emission through the TSB region formed by deep donors produce leakage current paths. By combining the results on gateless HFETs and Schottky diodes, a new unified model of near-surface electronic states for the free surface and Schottky interface of AlGaN is proposed. It consists of a U-shaped surface state continuum and N-vacancy related near-surface discrete deep donors. The model can explain the observed large gate leakage and drain current collapse in AlGaN/GaN HFETs in a unified way. It is also shown that our novel Al_2O_3 passivation, when also used as a gate insulator, can completely suppress current collapse and gate leakage. © *2003 American Vacuum Society.* [DOI: 10.1116/1.1589520]

I. INTRODUCTION

Being stimulated by recent explosive success of nitride based lasers and light emitting diodes in blue and ultraviolet regions, electronic devices such as AlGaN/GaN heterostructure field effect transistors (HFETs),[1–3] high-power metal–semiconductor field effect transistors (MESFETs),[4] and power rectifiers[5] have also made remarkable progress in recent years, resulting in unprecedented high power performances in microwaves and millimeter wave regions. Many workers believe that the AlGaN/GaN HFET will become the key device in the next-generation high frequency power electronics. Unfortunately, however, these devices still suffer from problems such as $I-V$ dispersion, drain current collapse,[6–11] gate- and drain-lag,[12] and large gate leakage currents[13,14] whose mechanisms are not well understood. There is experimental evidence which empirically indicates that they are related to ways of surface preparation and surface passivation, and therefore to the presence of surface states. However, it is difficult why these phenomena take so drastically in GaN-based devices as compared with GaAs-based devices such as AlGaAs/GaAs HFETs whose surfaces are characterized by equally or even higher densities of sur-

face states. Previous studies on these issues have been done in most cases on completed HFETs devices having gates schematically shown in Fig. 1(a), from the practical viewpoints. In gated devices, however, it is difficult to decide whether problems arise from the gated or ungated portion of the device.

As a new attempt to clarify the mechanisms of drain current collapse and gate leakage currents in AlGaN/GaN HFETs, the purpose of this article is to investigate the electrical properties of the ungated portion and Schottky-gated portion of the device separately, as schematically shown in Figs. 1(b) and 1(c), using a gateless HFET structure and an AlGaN Schottky diode structure. Use of a gateless FET structure for current transport study was done first by our group on sulfur passivation of GaAs a long time ago,[15] and this technique was shown to be extremely powerful in correlating various surface processings with inner current transport.

The surface of the gateless device was subjected to H_2 and N_2 plasma treatments as typical cleaning processes. It was also subjected to SiO_2-based and Al_2O_3-based surface passivation processes, including our novel Al_2O_3-based surface passivation utilizing electron cyclotron resonance

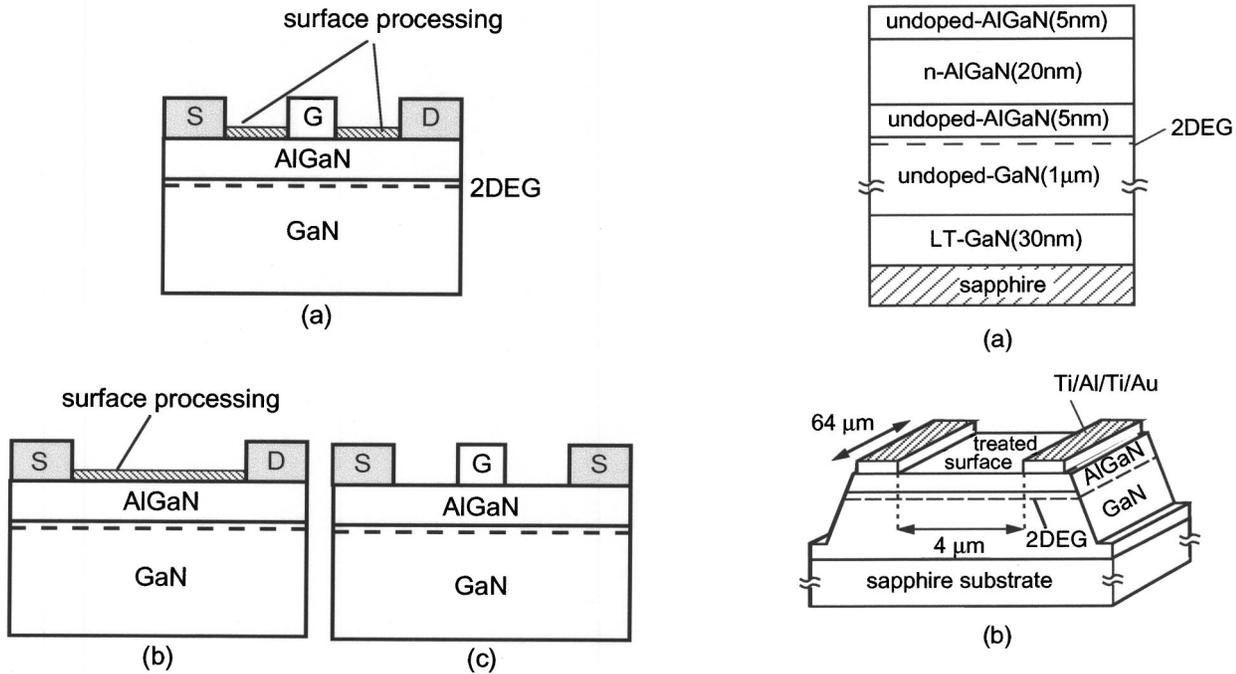[a] Electronic mail: hasegawa@rciqe.hokudai.ac.jp

FIG. 1. Schematic structures of (a) AlGaN/GaN HFET and its separation into (b) ungated and (c) gated portions.

(ECR) plasma oxidation of molecular beam deposited (MBD) Al film.[16]

dc $I-V$ curves of gateless HFETs were highly nonlinear due to virtual gating by surface states. After drain stress, air-exposed, H_2-plasma treated and SiO_2-deposited gateless HFETs showed an initial large-amplitude exponential current transient followed by a subsequent smaller, slow, and highly nonexponential response. The former was explained by emission from deep donors at $E_c - 0.37$ eV, and the latter by emission from surface states. A study of capture transients indicated the presence of stress-dependent capture barriers. An x-ray photoelectron spectroscopy (XPS) study indicated that deep donors are N-vacancy related. On the other hand, no current transients took place in N_2-plasma treated and Al_2O_3-passivated samples.

Temperature dependences of $I-V$ curves of Schottky diodes were extremely small and reverse currents were anomalously large. They were explained by thermionic field emission through the "thin surface barrier" formed by deep donors (TSB model).[17]

By combining the results on gateless HFETs and Schottky diodes, a new unified model of near-surface electronic states for the free surface and Schottky interface of AlGaN is proposed. The model involves a U-shaped surface state continuum and N-vacancy related near-surface discrete deep donors.[18] The model can explain the observed large gate leakage and drain current collapse in AlGaN/GaN HFETs in a unified way. It is also shown that our novel Al_2O_3 passivation, when also used as a gate insulator, can completely suppress current collapse and gate leakage.
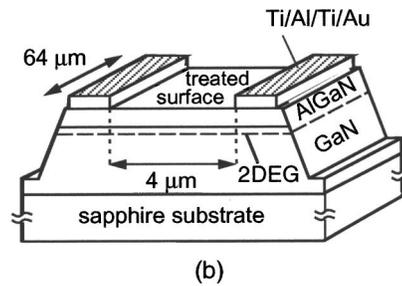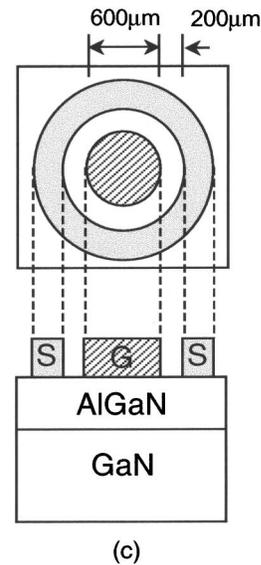
FIG. 2. Structures of (a) the wafer used in this study, (b) a gateless HFET device for study of the ungated portion, and (c) a Schottky diode for study of the gated portion.

II. EXPERIMENT

AlGaN/GaN wafers typically used for fabrication of HFETs were used in this study. Their structure is shown in Fig. 2(a). It had a structure of $Al_{0.28}Ga_{0.72}N$ (5 nm)/n^+-$Al_{0.28}Ga_{0.72}N$ (20 nm)/$Al_{0.28}Ga_{0.72}N$ (5 nm)/ undoped-GaN (1 μm) grown on sapphire substrates by metalorganic vapor phase epitaxy (MOVPE). The Hall mobility and sheet carrier density were 900 cm^2/V s and 1.1 $\times 10^{13}$ cm^{-2} at room temperature, respectively. At 2 K, the samples showed clear Shuvnikov−de Haas (SdH) oscillation

in magnetoresistance characteristics, and the electron concentration determined from the Landau plots of the oscillation was in good agreement with the value obtained by the Hall measurement at the same temperature. These results clearly indicated the existence of two-dimensional electron gas (2DEG) at the AlGaN/GaN heterointerface.

The actual structure[19] of the gateless HFET used for characterization of the ungated portions is shown in Fig. 2(b). It had a 2DEG channel width of 64 μm and a drain-source spacing of 4 μm. The sample fabrication process consisted of the mesa isolation by UV light-assisted KOH wet etching and the ohmic metallization for drain and source electrodes by alloying a Ti/Al/Ti/Au (20/80/20/50 nm) structure at 800 °C for 1 min in N_2 ambient. Although the present device is a two-terminal device, electrodes are called source and drain electrodes in this article so that the results on the gateless device can be correlated with behavior of the gated device. The drain is positively biased, and the voltage and current are called the drain voltage, V_{DS}, and drain current, I_{DS}, respectively.

The air-exposed surface of the gateless HFET was subjected to various surface processing. As typical surface processing for removal of native oxide prior to other processes such as gate metallization and passivation, H_2-plasma treatment, and N_2-plasma treatment, both excited by an electron-cyclotron-resonance (ECR) source, were investigated. It should be noted that these plasma species, especially H_2 plasma, are often used for dry etching of GaN-related materials. Both plasma treatments were applied for 1 min at 200 °C under ECR plasma excited at a microwave frequency of 2.75 GHz and a power of 50–100 W with gas flow rates of 5–10 sccm.

Attempts to passivate the air-exposed AlGaN surface of the gateless HFET were also made. Since it is widely known that drain current collapse takes place in a pronounced way in SiO_2-passivated devices, a SiO_2 film formed by the standard plasma chemical vapor deposition process using SiH_4 and N_2O on the HF treated AlGaN surface was chosen as the test passivation structure to clarify the collapse mechanism. It has been also reported that Si_3N_4-passivation significantly reduces the current collapse.[6–11] In this study, our novel Al_2O_3 passivation process[16] was investigated as an attempt to achieve further improvements. The sequence of formation of a high quality Al_2O_3 film on the AlGaN surface consisted of the following steps, and each step was carried out one after another in an ultrahigh vacuum (UHV) multichamber system without breaking vacuum. (1) N_2-plasma treatment of the AlGaN surface as described above. (2) Molecular beam deposition (MBD) of a 3-nm-thick Al layer at room temperature in the molecular beam epitaxy (MBE) chamber using the Al Knudsen cell at a deposition rate of ~0.01 nm/s. (3) UHV annealing at 700 °C for 10 min in the UHV annealing chamber. (4) Oxidation of the top Al layer by irradiation of O_2 plasma for 5 min in the ECR plasma chamber. (5) Annealing at 700 °C for 10 min in the UHV annealing chamber.

dc $I_{DS}-V_{DS}$ measurements of gateless HFETs were performed using an HP 4156A semiconductor parameter ana-

lyzer and current transients were measured using a pulse generator (NF Electronic WF-1944) and a digital oscilloscope (Tektronics TDS-3014).

The chemical properties of AlGaN surfaces after surface processing were characterized by *in situ* x-ray photoelectron spectroscopy (XPS) using a Perkin Elmer PHI 1600C system with a spherical capacitor analyzer and a monochromated Al $K\alpha$ x-ray source ($h\nu$=1486.6 eV). The samples after various surface processings in the ECR chamber were transferred to the XPS chamber without breaking the UHV condition, using a UHV transfer chamber.

For investigation of the gated portion, a ring-shaped Au/Ni Schottky structure shown in Fig. 2(c) was used. Detailed forward and backward Schottky current transport measurements were made for various values of temperature, T, using an HP 4156A semiconductor parameter analyzer.

III. EXPERIMENTAL RESULTS AND DISCUSSION

A. dc $I-V$ characteristics of gateless HFETs

dc $I_{DS}-V_{DS}$ curves of gateless HFETs having an air-exposed initial surface and surfaces subjected to various surface processing are summarized in Fig. 3(a). In spite of an ungated structure, all the curves showed the presence of the linear and saturation regions of currents similarly to those of the gated device. One possible mechanism of current saturation is the velocity saturation. However, the average electric field strength is too small to expect significant velocity saturation effect in such a long gate device.[20,21] Our interpretation is that it is due to the presence of strong Fermi level pinning by surface states which tends to fix the surface potential at a particular position, and makes the entire surface behave like a virtual gate. In fact, data could be reasonably well fitted to the theoretical dc $I_{DS}-V_{DS}$ curves based on the gradual channel approximation. This gave a surface Fermi level position of $E_{FS}=E_c-1.4$ eV for the initial air-exposed sample after taking account of the polarization effect.[22,23] The position is far away from the flatband. However, it is not so much surprising because it is similar to the case of the air-exposed AlGaAs surface with a high density of surface states.

After various surface processing, significant changes took place in $I_{DS}-V_{DS}$ characteristics, as seen in Fig. 3(a). After the H_2-plasma treatment and SiO_2 passivation, significant current reduction took place. On the other hand, current increased slightly after the N_2-plasma treatment and Al_2O_3 passivation. Analysis of the $I_{DS}-V_{DS}$ curves indicated that the observed current change is not due to mobility change, but caused by shifts of the effective flatband voltage in all cases. For example, the position of the surface Fermi level was shifted downward to lie at $E_c-1.7$ eV after the H_2-plasma treatment, and it is shifted upward to $E_c-1.2$ eV after the N_2-plasma treatment, respectively. The result roughly indicates a corresponding increase and decrease of the surface state density.
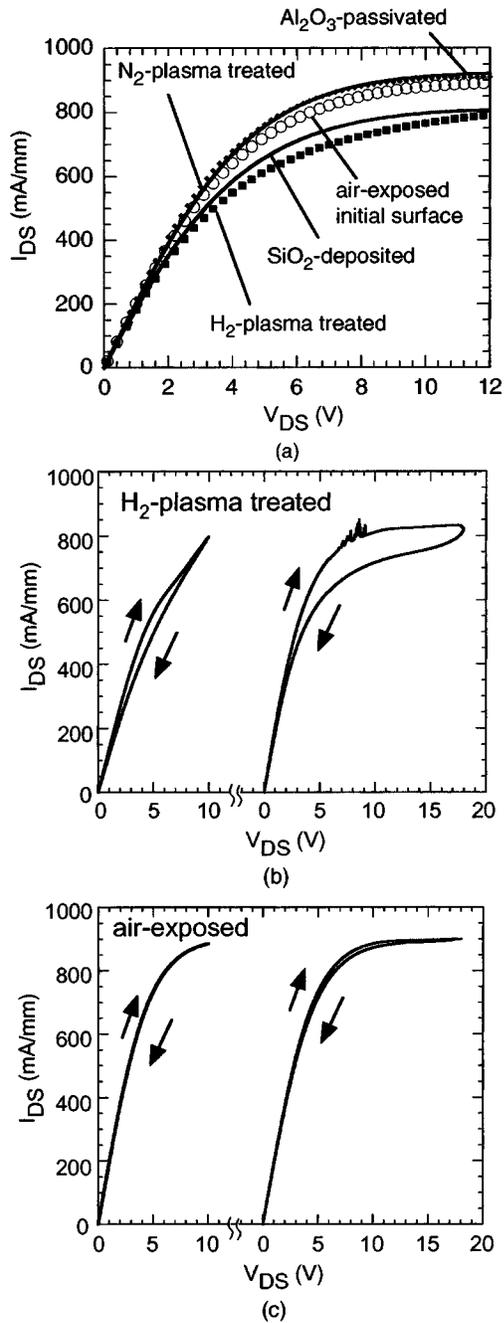
FIG. 3. (a) $I_{DS}-V_{DS}$ characteristics of the gateless HFET after various surface processing, (b) hysteresis behavior of $I-V$ curves observed after the H_2-plasma treatment, and (c) hysteresis behavior of $I-V$ curves observed in the air-exposed sample.
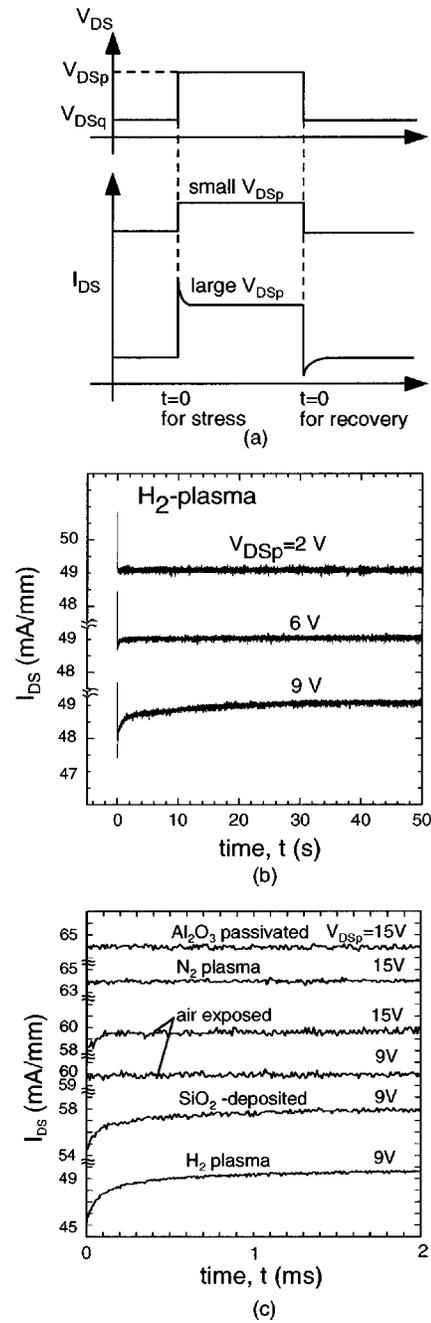

FIG. 4. (a) Schematic pulse wave forms for measurement of drain current transients of the gateless HFET, (b) recovering transient observed in the H_2-plasma sample at room temperature for three values of V_{DSp}, and (c) current transient in a shorter time scale for various samples.

Furthermore, H_2-plasma treated and SiO_2-passivated samples exhibited hysteresis in the dc $I-V$ curve as shown in Fig. 3(b) for the H_2-plasma treated sample. The magnitude of hysteresis depended strongly on the sweep range and the sweep rate of the drain voltage. The air-exposed sample also showed a very small hysteresis, as shown in Fig. 3(c), which became visible only for the drain voltage sweep larger than 15 V. On the other hand, no hysteresis was observed after N_2-plasma treatment and Al_2O_3 passivation. Thus H_2-plasma treatment and SiO_2-passivation introduce some deep states near the sample surface.

B. Pulsed *I–V* characteristics of gateless HFETs

Current transient measurements, simulating the drain current collapse under drain stress, were made using the pulse wave forms schematically shown in Fig. 4(a). The quiescent bias, V_{DSq}, was kept at 0.5 V in the linear region of the dc $I_{DS}-V_{DS}$ curve, and a drain-stress positive voltage with a variable peak value of V_{DSp} was applied for a duration time of $T_p = 50-300$ s. Then, the current transients during and after the voltage pulse were measured.

The observed current transient wave forms are schemati-

cally shown also in Fig. 4(a). When V_{DSp} was small, I_{DS} increased in a square fashion and came back to the original value at the quiescent bias at the finish of the stress pulse. However, when V_{DSp} was increased and entered into the saturation region of the dc $I_{DS}-V_{DS}$ curve, some samples started to show a current reducing transient during stress and a downward overshoot of currents at stress finish, followed by slow recovering transients.

Since recovering transients usually correspond to emission of carriers from deep traps, and provide important information on the properties of the traps, we first paid attention to recovering transients. The measured transient obtained on a H_2-plasma sample at room temperature is shown in Fig. 4(b). This recovery transient had a highly nonexponential long tail of several tens of seconds. However, the dominant part of the recovering transient was found to be a large-amplitude exponential-looking transient in the submillisecond range. To show this, the observed current transients at room temperature that were measured in the millisecond time range are summarized in Fig. 4(c). The transient amplitude was the largest in the H_2-plasma sample, and the SiO_2-passivated sample gave the second largest amplitude. In the air-exposed sample, transient became visible only at $V_{DSp}=15$ V. On the other hand, up to $V_{DSp}=15$ V or even higher, no transients of downward current overshoot and subsequent recovery were observed in the N_2-plasma sample and in the Al_2O_3-passivated sample.

An example of logarithmic plots of the initial fast current transients in sub-ms range is shown in Fig. 5(a) for the SiO_2-passivated sample. Although the data are rather noisy, the result confirms that the dominant fast transient is indeed an exponential one with a single time constant. The same was confirmed in other samples which showed transients. The measured temperature dependences of the time constants are plotted in Fig. 5(b) as a function of the inverse temperature for the H_2-plasma treated, SiO_2-passivated, and air-exposed sample. Vertical error bars for time constants correspond to fitting errors. It was also confirmed that the transient amplitudes depend on the value of V_{DSp} but the time constant itself is independent of V_{DSp}. As seen in Fig. 5(b), the same Arrhenius-type temperature dependence with an activation energy, ΔE, of 0.37 eV was observed for these three samples, strongly indicating that the dominant parts of the transients in these samples are caused by the same trap, although the surface processing was different. Assuming that the transient is due to electron emission from a deep donor to the AlGaN conduction band, the time constant is given by

$$\tau = (N_c \sigma_n v_{thn})^{-1} \exp\left(\frac{\Delta E}{kT}\right) \quad (1)$$

in the standard notation. Using $N_c = 2.2 \times 10^{18}$ cm^{-3} and $v_{thn} = 6 \times 10^6$ cm/s at 300 K for $Al_{0.28}Ga_{0.72}N$, an electron capture cross section, σ_n, of 1.2×10^{-16} cm^2 was obtained.

Thus a deep donor with the signature plot shown in Fig. 5(b) plays a dominant role in the current transients observed in the three types of samples. On the other hand, subsequent small-amplitude, slow, and highly nonexponential responses
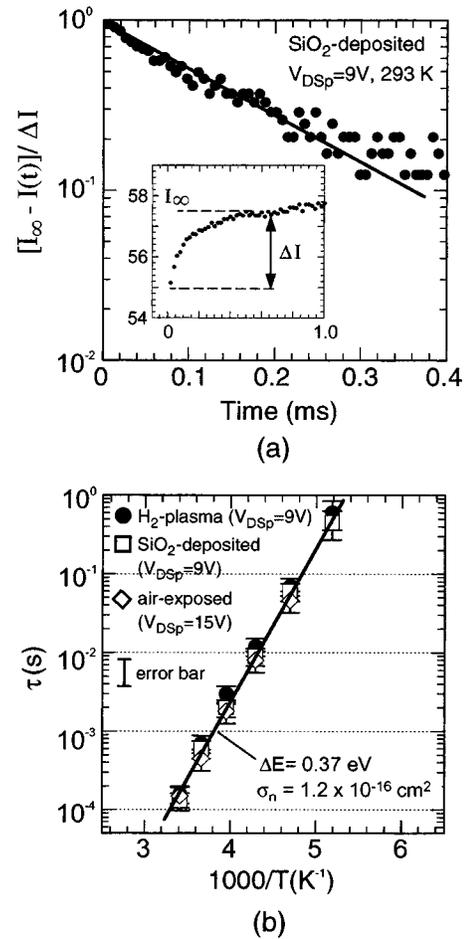

FIG. 5. (a) Logarithm plots of the fast current transient of the SiO_2-passivated sample at 293 K, and (b) Arrhenius plots of the time constant of "fast" transient current for three samples.

in these samples seem to be typical of electron emission from a surface state continuum which includes a wide range of time constants.

The fact that dc current saturation can be explained in terms of virtual gating, and the fact that amplitudes of the current transient increased with V_{DSp}, strongly suggest that the electron emission takes place at the drain side of the gateless FET. In order to directly confirm this, a special sample shown in Fig. 6(a) was prepared, where only a half of the surface was subjected to H_2 plasma and other half remained as an air-exposed surface covered by a thick photoresist. This sample showed asymmetric transients shown in Fig. 6(a) corresponding to whether the H_2-plasma treated surface becomes the drain side or not. The result directly indicates that transients indeed take place at the drain edge.

The current transients during the stress pulse were also measured. They should correspond to electron capture by the deep trap and surface states. Examples of measured wave forms taken on the H_2-plasma sample at room temperature are shown in Fig. 6(b). They show again predominant fast transients followed by slow transients, quantitatively in agreement with the above interpretation of carrier capture by the deep trap and surface states. In fact, the logarithm plots
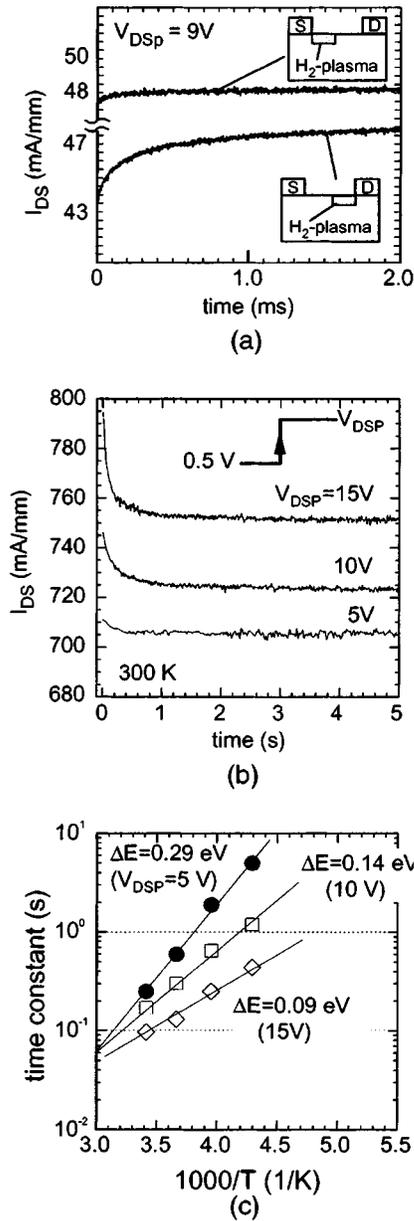
FIG. 6. (a) Transients observed in a special sample with partial H_2-plasma treatment, (b) capture transient curves observed in the H_2-plasma sample, and (c) temperature and stress dependences of the capture time constant.

FIG. 7. (a) Ga $3d$ and (b) N $1s$ XPS core-level spectra of plasma-treated AlGaN surfaces.

of the initial parts confirmed their exponential nature. However, the observed capture transients are very different from the standard capture behavior of a deep level in the following three points. (1) The capture time constant of the initial exponential transient is much longer than that of the corresponding emission transient, although the opposite takes place in the usual cases. (2) This time constant is stress voltage-dependent, as can be seen in Fig. 6(b). (3) This time constant is also temperature-dependent as summarized in Fig. 6(c) in the form of the Arrhenius plots. These results strongly indicate that a stress-dependent capture barrier exists in the capture process near the drain edge of electrons by the 0.37 eV donor and the surface state continuum.
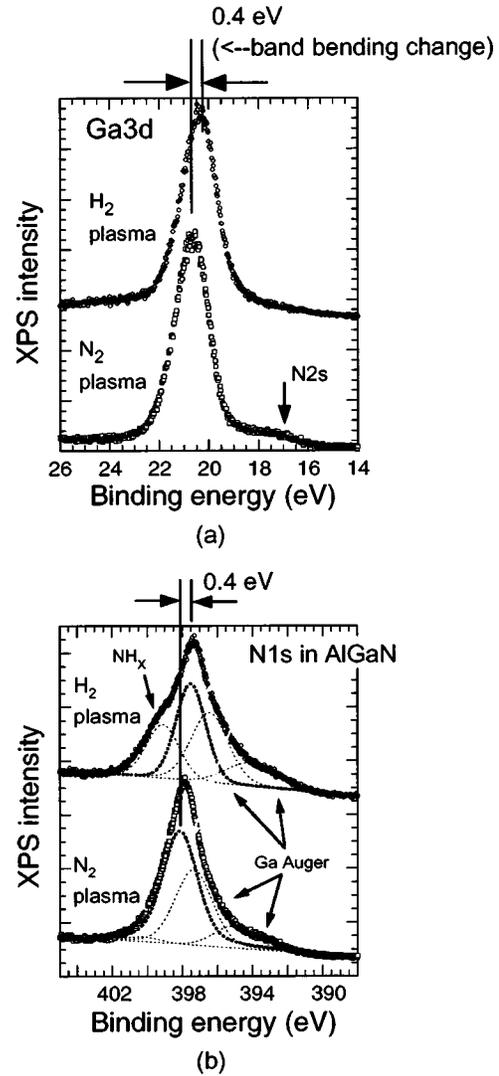
C. XPS analysis of plasma treated surfaces

In order to obtain information on the chemical origin of the dominant 0.37 eV deep donor, *in situ* XPS measurements were carried out on the H_2-plasma and N_2-plasma samples where complications introduced by insulator formation in passivated samples can be avoided. The measured XPS spectra taken on the AlGaN surface just after H_2-plasma and N_2-plasma treatments are compared in Figs. 7(a) and 7(b) for Ga $3d$ and N $1s$ core-level peaks, respectively. In these figures, photoemission from the AlGaN surface was detected at an electron escape angle of 10° to make it surface-sensitive.

The N $1s$ core-level spectra of the N_2-plasma treated sample were deconvoluted into three components, i.e., the component corresponding to N atoms in AlGaN and two other components corresponding to Ga Auger peaks. On the other hand, an additional shoulder peak appeared at around 399 eV in the N $1s$ core-level spectrum of the H_2-plasma treated sample. This corresponds to the binding energy of the N–H_x bond.[24] After this deconvolution analysis, the values

TABLE I. Result of XPS analysis of near-surface stoichiometry on plasma treated samples.

	$\dfrac{[Al]}{[Al]+[Ga]}$	$\dfrac{[N]}{[Al]+[Ga]}$
N_2 plasma	0.28	1.04
H_2 plasma	0.33	0.79

FIG. 8. (a) Measured forward and reverse $I-V-T$ characteristics and (b) $C-V$ curves of a Au–Ni/AlGaN Schottky diode.

of integrated intensity ratio of the Ga, Al, and N peaks were compared with those of the reference AlGaN sample taken at the escape angle of 70°. The surface of the reference sample was treated by warm NH_4OH (Ref. 25) which was found to be the best remover of native oxide without plasma damage. The result is summarized in Table I. It was found that the N_2-plasma treated surface maintains the surface stoichiometry remarkably well. On the other hand, it was also found that the V/III ratio of the AlGaN surface after the H_2-plasma treatment was far below unity, strongly indicating depletion of N atoms near the surface.

The above result provides the following interpretation. Namely, during the H_2 plasma treatment, highly active hydrogen plasma species such as hydrogen radicals react with the AlGaN surface to form volatile NH_x products. This leads to the depletion of N atoms and the formation of Ga and Al clusters at the topmost AlGaN surface. Such a surface reaction process is thus most likely to introduce N vacancies and related defects in the surface region of AlGaN.

Existence of the same 0.37 eV donor defect was also seen in the SiO_2-passivated sample and air-exposed samples according to the current transient study, and this has to be also explained. As for the SiO_2 deposition, subcutaneous oxidation is inevitable, and this leads to escape of N atoms in the NO_x form as well as to the partial formation of Ga oxide. Escape of N atoms will introduce N vacancies and related defects in the near-surface region of AlGaN. It is also expected that a similar situation takes place by air exposure of the surface due to natural oxidation.

Another point which is noted in Figs. 7(a) and 7(b) is that the peak positions of Ga $3d$ and N $1s$ spectra of the H_2 plasma treated sample are shifted toward the lower binding energy side by the same amount of 0.4 eV with reference to those of the N_2-plasma treated sample. This indicates that the upward band bending is larger on the H_2-plasma treated surface by 0.4 eV than on the N_2-plasma treated surface. This result is consistent with the difference of Fermi level pinning positions of $(1.7-1.2=)$ 0.5 eV inferred from the analysis of dc saturation currents of the gateless HFET.

Thus the most likely candidate for the observed 0.37 eV deep donor is the N vacancy, or some complex related to N vacancy. There are some previous works related to N vacancy in GaN and AlGaN. For example, Hughes *et al.*[26] suggested that the N vacancy dominates the surface structure. Previous experimental and theoretical studies also indicated that the N vacancy acts as a donor.[27–30] As for the energy location of the N-vacancy donor, a theoretical calculation by Neuberger and Van de Walle[28] indicated that it forms a shal-
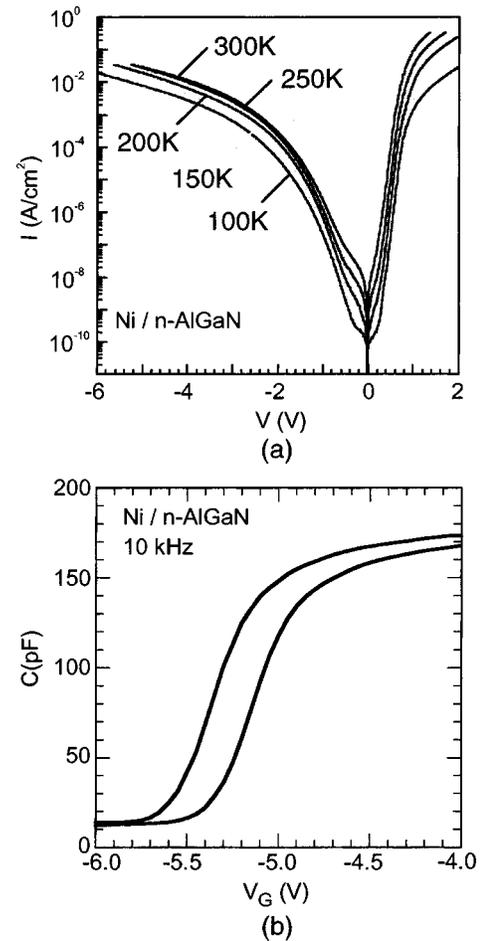
low donor. On the other hand, a recent theoretical calculation by Yamaguchi and Junnarkar[30] predicted that the N vacancy defects can form *s*-like deep donor levels at around E_c -0.4 eV within the gap of GaN and AlGaN. The latter calculation seems to agree excellently with the present result and interpretation.

D. *I–V* and *C–V* characteristics of AlGaN Schottky diodes

In order to understand the mechanism of large gate leakage currents in AlGaN/GaN HFETs, forward and reverse $I-V$ characteristics of the Au/Ni Schottky diode shown in Fig. 2(c) were measured in detail at various temperatures. The result is summarized in Fig. 8(a). If we pay attention only to the forward current at room temperature, and apply the conventional thermionic emission (TE) model to the data, as is usually done, the barrier height and the ideality factor are evaluated as $\phi_B^{TE}=0.96$ eV and $n^{TE}=1.53$, respectively. However, the measured $I-V$ curves deviate very much from the prediction of the TE model. Main points of deviation are the following. (1) Forward $I-V$ curves show small parallel shifts with temperature, indicating that the effective ideality factor increases as the temperature is lowered. (2) Reverse

currents under small reverse bias do not show $\exp \times (-\phi_B^{\text{TE}}/kT)$ dependence at all, thereby deviating from the thermionic emission transport by many orders of magnitudes. (3) Reverse currents show an anomalously sharp increase as the reverse bias is increased to large values. Currents almost reach the levels of the forward currents.

For example, the room temperature reverse current at -6 V is already eight orders of magnitude larger than the prediction of the reverse saturation current by the TE model, and the deviation further increases as the temperature is lowered. Thus the current transport mechanism cannot be the TE mechanism.

On the other hand, the above features of $I-V$ characteristics are very similar to those of GaN Schottky diodes which we discussed recently[17] where the behavior was explained by the thin surface barrier (TSB) model. In this model, the width of the Schottky barrier is very much thinned down due to the presence of a high density of unintentional surface donors, and electrons tunnel though this barrier in both forward and reverse direction in the form of a Gaussian beam by the mechanism of the thermionic field emission (TFE) or the field emission (FE) mechanism,[31] depending on the temperature. As for the origin of the surface donors, it has been proposed that bombardment with high-energy metal atoms produce N-vacancy-related deep donor traps.[17] The data in Fig. 8(a) strongly indicate that the same mechanism is at work in a more drastic way in the present AlGaN Schottky barrier.

The measured capacitance–voltage ($C-V$) curves of the Schottky diode are shown in Fig. 8(b). The observed bias-dependence of the capacitance is typical of the Schottky diode having a 2DEG channel underneath. However, the diode showed hysteresis behavior, indicating the presence of deep levels. It is highly likely that hysteresis is caused again by the N-vacancy related deep traps produced by surface bombardment with high energy metal atoms.

IV. MODEL FOR ELECTRONIC STATES AND MECHANISMS OF GATE LEAKAGE AND CURRENT COLLAPSE

A. Unified model for electronic states at free surfaces and Schottky interfaces of AlGaN

On the basis of the experimental results, a new unified model shown in Fig. 9(a) with a common effective surface state density distribution shown in Fig. 9(b) is proposed for near-surface electronic states at free surfaces and a Schottky interface of AlGaN. It consists of a surface state continuum and a discrete peak due to near-surface bulk donors projected onto the surface.

Similarly to other III–V semiconductors,[32] a U-shaped high density surface state continuum is formed which pins the surface Fermi level near the charge neutrality level (CNL). For the energy distribution of the surface density, $N_{\text{ss}}(E)$, the following formula can be used in accordance with the disorder-induced gap state (DIGS) model.[32]
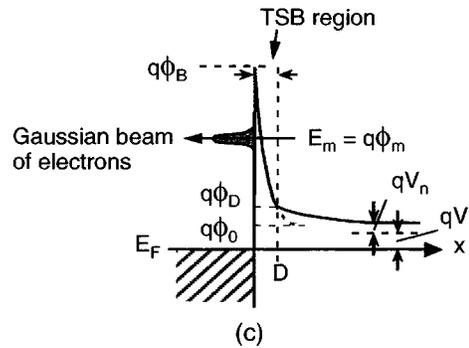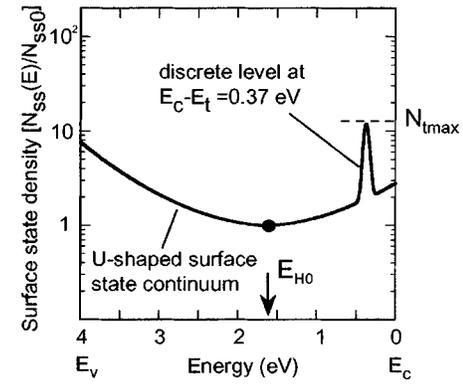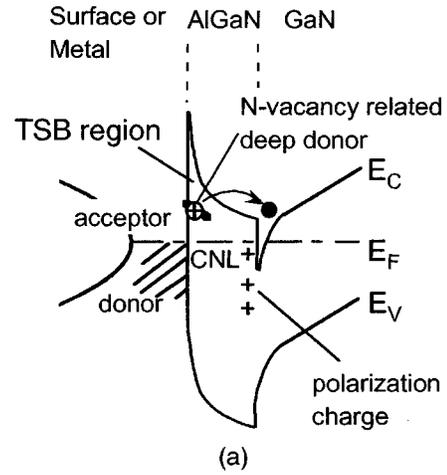

FIG. 9. (a) New unified model for near-surface electronic states of AlGaN, (b) a combined distribution of state density, and (c) the TSB model for current transport at the Schottky interface.

$$N_{\text{ss}}(E) = N_{\text{ss0}} \exp\left(\frac{|E - E_{\text{HO}}|}{E_0}\right)^{n_j}, \tag{2}$$

where N_{ss0} is the minimum surface state density and E_{HO} is the energy position of the charge neutrality level. E_{0j} and n_j determine the distribution shape with $j=d$ for donor-like gap states located below E_{HO}, and $j=a$ for acceptor-like gap states above E_{HO}. The position of E_{HO} is determined by the mean hybrid orbital energy of the semiconductor crystal in the tight-binding context.[32] Using the branch point data com-

piled by Kampen and Mönch,[33] its position for $Al_xGa_{1-x}N$ may be deduced by the following formula based on linear interpolation.

$$E_{HO}(eV) = E_V + 2.37 + 0.60x. \qquad (3)$$

In addition to the U-shaped continuum, high-density deep donors related to N vacancies are created near the surface at $E_c - 0.37$ eV as shown in Fig. 9(b). Its density strongly depends on details of surface processing such as plasma treatments for oxide removal and dry etching, passivation, and metal deposition. Due to Fermi level pinning near E_{HO} both at free surfaces and at the Schottky interface, these deep donors are ionized, supplying electrons to 2DEG together with those due to shallow donors and intrinsic and piezoelectric polarization.[22,23] This produces a thin surface barrier (TSB) region shown in Fig. 9(c), as we recently proposed for GaN Schottky diodes.[17]

## B. Mechanism of large gate leakage currents

In the case of the Schottky interface, the TSB region gives rise to a TFE/TE path for current transport, producing large leakage currents in HFETs. In the case of the forward currents, the transport is mainly the TFE mechanism and the ideality factor for forward currents, n_F, is given by the following formula.[31]

$$n_F = \frac{E_{00}}{kT} \coth\left(\frac{E_{00}}{kT}\right), \qquad (4a)$$

with $\quad E_{00} = (qh/4\pi)(N_{DS}/m^*\varepsilon_s)^{1/2}, \qquad (4b)$

where q is the electronic charge, h is Planck's constant, m^* is the effective mass, ε_s is the permittivity of semiconductor, and N_{DS} is the density of unintentional surface donors. The measured values of n_F are compared in Fig. 10(a) with the theoretical curves calculated from Eqs. (4a) and (4b). The measured values of n_F could be very well fitted into the theoretical curve. The donor concentration N_{DS} obtained by fitting is 8×10^{18} cm^{-3}, and this is much larger than the value of the shallow donor concentration of $N_D = 3 \times 10^{17}$ cm^{-3} of the sample used in the experiment.

Using the value of N_{DS} thus obtained, theoretical curves of forward and reverse currents for the present AlGaN Schottky diode were calculated as a function of temperature, T, using the approximate formulas derived for GaN Schottky barriers having a rectangular distribution of surface donors.[17] The results are compared with experimental data in Figs. 10(b) and 10(c) for forward and reverse currents, respectively. It should be noted that unnatural kinks in the theoretical curves for reverse bias are artifacts due to connection of approximate TFE curves at lower biases and approximate FE curves at higher biases. In spite of these approximate natures, the calculation has reproduced the experimental $I-V-T$ curves not only qualitatively, but also semiquantitatively in both forward and reverse directions. The discrepancy under small bias seems to be due to the assumption of a simple rectangular distribution used to obtain analytical formulas.[17]
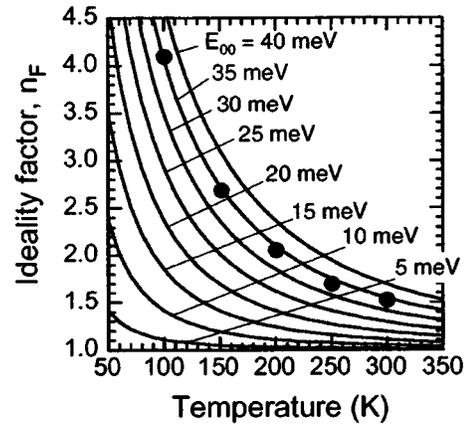
(a)
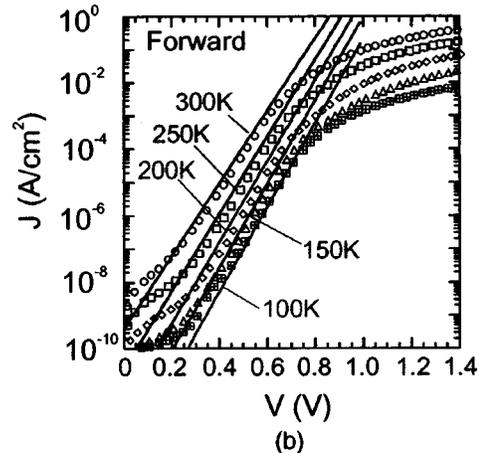
(b)
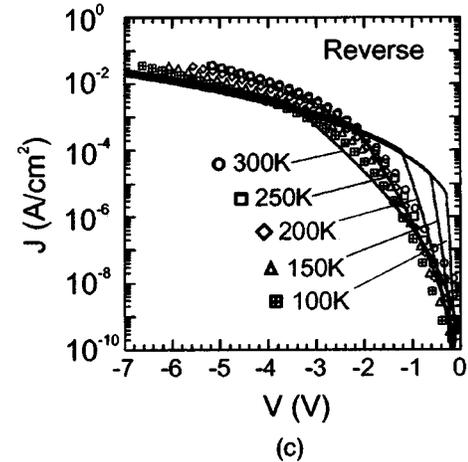
(c)

FIG. 10. (a) Comparison of the ideality factor between theory and experiment, and calculated and experimental $I-V-T$ characteristics for (b) forward and (c) reverse bias.

C. Mechanism of drain current collapse

The drain current collapse, or $I-V$ dispersion, is a serious phenomenon in AlGaN/GaN HFETs in high power applications. The phenomenon is schematically shown in Fig. 11(a) where drain currents in the $I-V$ curves measured at dc are very much reduced when they are measured under large amplitude high-frequency gate swings. In the actual power applications, the device is switched between on- and off-states
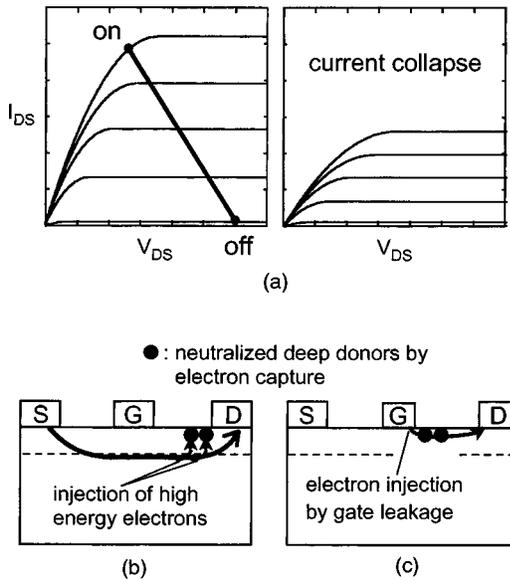
FIG. 11. (a) Schematic representation of drain current collapse. Our models for current collapse (b) under drain stress and (c) under gate stress.

along the load line, and reduction of on-state currents leads to serious performance degradation in power applications. Subsequent pulsed and ramped measurements by the previous workers have shown that the reduction of the drain current takes place under dc or pulsed bias stress under on-state condition in the saturation region (drain stress) as well as under off-state condition in the region of channel pinch off by dc or pulsed gate bias (gate stress). Therefore characterization of current collapse has been done under drain stress[6,7,11] and under gate stress.[6–10]

The above behavior is, however, very surprising from a naive point of near surface trapping by deep states such as encountered in drain current drift in III–V metal–insulator–semiconductor field effect transistors (MISFETs). This is because if the on-state drain stress causes capture of 2DEG channel electrons by deep levels, thereby reducing channel currents, then the off-state gate stress should give emission of electrons back to the channel, leading to an increase of the on-state drain current rather than the observed decrease. Thus the model of current collapse should be capable of this mysterious behavior in a consistent way.

Our explanation of current collapse is shown in Fig. 11(b) and 11(c) for the cases of drain-stress and gate-stress, respectively. As shown in Fig. 11(b), injection of high-energy electrons takes place from the 2DEG channel into the AlGaN region near the drain edge under the application of a large drain-stress voltage V_{DSp}. Due to electron injection, near-surface traps and surface states are filled near the drain edge, reducing 2DEG density and expanding the depletion width. This causes current collapse. Then, after switching back the drain voltage, electrons in these states are emitted, leading to recovery transients.

To confirm such a picture, a computer simulation of measured current recovery transients was attempted using the combined state distribution shown in Fig. 9(b). For the dis-

crete near-surface donor level, a donor-type Gaussian peak situated at the measured energy position of 0.37 eV was assumed, treating the near-surface bulk deep donors as projected surface states for simplicity. For the U-shaped distributions, Eq. (2) was used and a value of $E_{HO} = E_c - 1.6$ eV was used according to Eq. (3) for $Al_{0.28}Ga_{0.72}N$. The transients were calculated using the following equation instead of the stretched exponential form used previously.[11]

$$N_{emit}(t) = \int N_{ss}(E)\left[1 - \exp\left(-\frac{t}{\tau(E)}\right)\right]dE. \qquad (5)$$

After many trials, excellent fits were obtained by assuming a combined state density distribution shown in Fig. 12(a), and the results of fitting are shown in Figs. 12(b) and 12(c). As seen in Fig. 12(b), the dominant fast transient is due to the electron emission from the discrete level. The total density of the 0.37 eV level was determined to be 5×10^{11} cm^{-2}. On the other hand, as shown in Fig. 12(c), a slow increase in current at a longer time regime is due to the emission from continuous surface states that have a wide range of time constant.

The observed presence of the stress-dependent capture barrier is also consistently explained in terms of injection of high energy electrons into the AlGaN region from the 2DEG channel. The activation energy values shown in Fig. 6(c) can be interpreted as the energy difference between the bottom of the AlGaN conduction band at the surface and the quasi-Fermi level of high-energy electrons in the AlGaN layer. As the stress magnitude is increased, more and more electrons are injected into the AlGaN layer, and the band bending is rapidly reduced, leading to stress dependent capture barrier heights.

As for the behavior under the gate stress, the present gate-less HFET structure cannot provide experimental data. However, from the large leakage currents and its mechanism discussed for the Schottky diode, we propose the mechanism shown in Fig. 11(c). Although the channel current from the source is completely pinched off, there exists a large leakage current from the gate into the AlGaN layer through the TFE/FE mechanism underneath the gate. Such a gate injection of electrons will fill up the 0.37 eV traps and surface states in the region near the gate on the drain side, causing virtual gating by these near-surface electronic states.

Finally, in order to suppress such current collapse under drain stress and under gate stress completely, the N-vacancy related traps should be removed from the free surface and underneath the gate. The present study has shown that our Al_2O_3-passivation scheme including N_2-plasma surface treatment completely removes this trap as well as reduces surface states. The latter is based on the observed reduction of band banding mentioned previously. However, it may be difficult to completely suppress the formation of N-vacancies near the Schottky gate, since any of the metal deposition processes involves high energy metal ions except the special processes such as metal deposition by the wet electrochemical process[34] where we observed a significant reduction of reverse leakage in GaN Schottky diodes.
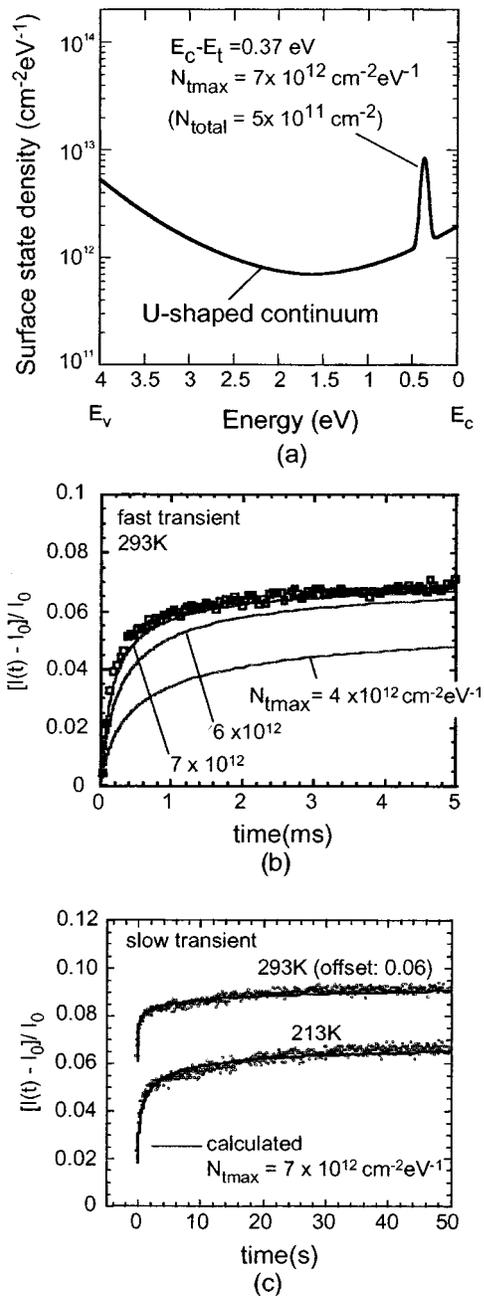
FIG. 12. (a) Surface state density distribution obtained from the fitting of the transient currents. The results of fitting (b) in a short time scale and (c) in a long time scale.

One practical solution to this problem is to utilize the Al_2O_3 also as the insulator for the insulated gate (IG) device as we proposed recently.[16] We demonstrated reduction of gate leakage by four to five orders of magnitude in comparison with the Schottky gate. As compared with a similar IG structure using Si_3N_4, Al_2O_3 offers a larger band gap, a lager conduction band offset with AlGaN, and a larger permittivity, making it a highly attractive "high k dielectric" to AlGaN. In fact, our latest ultrathin Al_2O_3–IG AlGaN/GaN HFETs with a submicron gate have been found completely collapse-free under drain and gate stress conditions, and exhibited the largest g_m of 120 mS/mm reported for the IG

AlGaN/GaN HFET device, as will be reported elsewhere.[35]

V. CONCLUSIONS

In order to clarify the mechanisms of drain current collapse and gate leakage currents in the AlGaN/GaN heterostructure field effect transistor (HFET), this article has investigated electrical properties of the ungated portion and Schottky-gated portion of the device separately, using a gateless HFET structure and an AlGaN Schottky diode structure under various surface processing. The main conclusions are listed below.

(1) dc I–V curves of gateless HFETs were highly nonlinear due to virtual gating by surface states.

(2) After drain stress, air-exposed, H_2-plasma treated and SiO_2-deposited gateless HFETs showed an initial large-amplitude exponential current transient followed by a subsequent smaller, slow, and highly nonexponential response. The former was explained by emission from deep donors at $E_c - 0.37$ eV, and the latter by emission from the surface state continuum.

(3) Capture transients during the stress period indicated the presence of stress-dependent capture barriers.

(4) An x-ray photoelectron spectroscopy (XPS) study indicated that 0.37 eV-deep donors are N-vacancy related.

(5) No current transients took place in N_2-plasma treated and Al_2O_3-passivated samples.

(6) Temperature dependences of I–V curves of Schottky diodes were extremely small and reverse currents were anomalously large. They were explained by the "thin surface barrier" (TSB) model where thermionic field emission and field emission through the TSB regions, formed by deep donors, provide leakage current paths.

(7) By combining the results on gateless HFETs and Schottky diodes, a new unified model of near-surface electronic states for the free surface and Schottky interface of AlGaN has been proposed. It consists of a U-shaped surface state continuum and N-vacancy related near-surface discrete deep donors. The model can explain the observed large gate leakage and drain current collapse in AlGaN/GaN HFETs in a unified way.

(8) A scheme of surface passivation and insulated gate structure using Al_2O_3, recently proposed by the authors, can completely suppress current collapse and gate leakage.

[1] Y.-F. Wu, B. P. Keller, P. Fini, J. Pusl, M. Le, N. X. Nguyen, C. Nguyen, D. Widman, S. Keller, S. P. Denbaars, and U. K. Mishra, Electron. Lett. **33**, 1742 (1997).
[2] N. X. Nguyen, M. Micovic, W.-S. Wong, P. Hashimoto, L.-M. McCray, P. Janke, and C. Nguyen, Electron. Lett. **36**, 468 (2000).

[3] S. T. Sheppard, K. Doverspike, W. L. Pribble, S. T. Allen, J. W. Palmour, L. T. Kehias, and T. J. Jenkins, IEEE Electron Device Lett. **20**, 161 (1999).

[4] R. Gaska, M. S. Shur, X. Hu, J. W. Yang, A. Tarakji, G. Simin, A. Khan, J. Deng, T. Werner, S. Rumyantsev, and N. Pala, Appl. Phys. Lett. **78**, 769 (2001).

[5] A. P. Zhang, J. W. Johnson, F. Ren, J. Han, A. Y. Polyakov, N. B. Smirnov, A. V. Govorkov, J. M. Redwing, K. P. Lee, and S. J. Pearton, Appl. Phys. Lett. **78**, 823 (2001).

[6] K. Kunihiro, K. Kasahara, Y. Takahashi, and Y. Ohno, Jpn. J. Appl. Phys., Part 1 **39**, 2431 (2000).

[7] X. Hu, A. Koudymov, G. Simin, J. Yang, M. A. Khan, A. Tarakji, M. S. Shur, and R. Gaska, Appl. Phys. Lett. **79**, 2832 (2001).

[8] B. Luo, J. W. Johnson, J. Kim, R. M. Mahandru, F. Ren, B. P. Gila, A. H. Onstine, C. R. Abernathy, S. J. Pearton, A. G. Baca, R. D. Briggs, R. J. Shul, C. Monier, and J. Han, Appl. Phys. Lett. **80**, 1661 (2002).

[9] T. Kikkawa, M. Nagahara, N. Okamoto, Y. Tateno, Y. Yamaguchi, N. Hara, K. Joshin, and P. M. Asbeck, IEDM Technical Digest 2001, p. 585.

[10] T. Mizutani, Y. Ohno, M. Akita, S. Kishimoto, and K. Maezawa, Phys. Status Solidi A **194**, 447 (2002).

[11] R. Vetury, N. Q. Zhang, S. Keller, and U. K. Mishra, IEEE Trans. Electron Devices **48**, 560 (2001).

[12] S. C. Binari *et al.*, IEEE Trans. Electron Devices **48**, 465 (2001).

[13] S. Rumyantsev *et al.*, J. Appl. Phys. **87**, 1849 (2000).

[14] S. Oyama, T. Hashizume, and H. Hasegawa, Appl. Surf. Sci. **190**, 322 (2002).

[15] H. Hasegawa *et al.*, J. Vac. Sci. Technol. B **5**, 1097 (1987).

[16] S. Ootomo, T. Hashizume, and H. Hasegawa, presented at IWN2002, Aachen, Germany, 2002 [Phys. Status Solidi C **0**, 90 (2002)].

[17] H. Hasegawa and S. Oyama, J. Vac. Sci. Technol. B **20**, 1467 (2002).

[18] H. Hasegawa, T. Inagaki, S. Ootomo, and T. Hashizume, presented at ISCS-02, Lausanne, Switzerland, 2002 (unpublished).

[19] T. Inagaki, T. Hashizume, and H. Hasegawa, Appl. Surf. Sci. (to be published).

[20] R. J. Trew, M. W. Shin, and V. Gatto, Solid-State Electron. **41**, 1561 (1997).

[21] B. E. Foutz *et al.*, J. Appl. Phys. **85**, 7727 (1999).

[22] O. Ambacher *et al.*, J. Appl. Phys. **85**, 3222 (1999).

[23] J. P. Ibbetson, P. T. Fini, K. D. Ness, S. P. Denbaars, J. S. Speck, and U. K. Mishra, Appl. Phys. Lett. **77**, 250 (2000).

[24] X. Y. Zhu, M. Wolf, and J. M. White, J. Vac. Sci. Technol. A **11**, 838 (1993).

[25] T. Hashizume *et al.*, Appl. Phys. Lett. **76**, 2880 (2000).

[26] G. H. Hughes, D. Korakakis, T. S. Cheng, A. V. Blant, N. J. Jeffs, and C. T. Foxon, J. Vac. Sci. Technol. B **16**, 2237 (1998).

[27] T. L. Tansley and R. J. Egan, Phys. Rev. B **45**, 10942 (1992).

[28] J. Neugebauer and C. G. Van de Walle, Phys. Rev. B **50**, 8067 (1994).

[29] P. Boguslauski, E. L. Briggs, and J. Bernholc, Phys. Rev. B **51**, 17255 (1995).

[30] E. Yamaguchi and M. R. Junnarkar, J. Cryst. Growth **189/190**, 570 (1998).

[31] F. A. Padovani and R. Stratton, Solid-State Electron. **9**, 695 (1966).

[32] H. Hasegawa and H. Ohno, J. Vac. Sci. Technol. B **4**, 1130 (1986).

[33] T. U. Kampen and W. Mönch, Appl. Surf. Sci. **117/118**, 388 (1977).

[34] T. Sato, S. Oyama, and H. Hasegawa, presented at ICPS-26, Edinburgh, UK, 2002 (unpublished).

[35] T. Hashizume and H. Hasegawa, presented at PCSI-30 as an invited paper, J. Vac. Sci. Technol. B, these proceedings.